RESEARCH ARTICLE

WILEY

Age-associated change in pyruvate metabolism investigated with hyperpolarized ^{13}C-MRI of the human brain

Biranavan Uthayakumar[1,2] | Hany Soliman[3] | Nadia D. Bragagnolo[2] |
Nicole I. C. Cappelletto[1,2] | Casey Y. Lee[1,2] | Benjamin Geraghty[1,2] |
Albert P. Chen[4] | William J. Perks[5] | Nathan Ma[5] | Chris Heyn[6] |
Ruby Endre[2] | Bradley J. MacIntosh[1,2,7] | Greg J. Stanisz[1,2,8] |
Sandra E. Black[7,9] | Charles H. Cunningham[1,2]

[1]Department of Medical Biophysics, University of Toronto, Toronto, Ontario, Canada

[2]Physical Sciences, Sunnybrook Research Institute, Toronto, Ontario, Canada

[3]Radiation Oncology, Sunnybrook Health Sciences Centre, Toronto, Ontario, Canada

[4]GE Healthcare, Toronto, Ontario, Canada

[5]Pharmacy, Sunnybrook Health Sciences Centre, Toronto, Ontario, Canada

[6]Radiology, Sunnybrook Health Sciences Centre, Toronto, Ontario, Canada

[7]Dr. Sandra Black Centre for Brain Resilience and Recovery, Hurvitz Brain Sciences Research Program, Sunnybrook Research Institute, Toronto, Ontario, Canada

[8]Department of Neurosurgery, Medical University, Lublin, Poland

[9]Department of Medicine (Neurology), University of Toronto, Toronto, Ontario, Canada

Correspondence

Charles H. Cunningham, Department of Medical Biophysics, University of Toronto. 2075 Bayview Avenue, Toronto, ON M4N 3M5, Canada.
Email: charles.cunningham@utoronto.ca

Abstract

In this study, hyperpolarized ^{13}C MRI (HP-^{13}C MRI) was used to investigate changes in the uptake and metabolism of pyruvate with age. Hyperpolarized ^{13}C-pyruvate was administered to healthy aging individuals ($N = 35$, ages 21–77) and whole-brain spatial distributions of ^{13}C-lactate and ^{13}C-bicarbonate production were measured. Linear mixed-effects regressions were performed to compute the regional percentage change per decade, showing a significant reduction in both normalized ^{13}C-lactate and normalized ^{13}C-bicarbonate production with age: $-7\% \pm 2\%$ per decade for ^{13}C-lactate and $-9\% \pm 4\%$ per decade for ^{13}C-bicarbonate. Certain regions, such as the right medial precentral gyrus, showed greater rates of change while the left caudate nucleus had a flat ^{13}C-lactate versus age and a slightly increasing ^{13}C-bicarbonate versus age. The results show that both the production of lactate (visible as ^{13}C-lactate signal) as well as the consumption of monocarboxylates to make acetyl-CoA (visible as ^{13}C-bicarbonate signal) decrease with age and that the rate of change varies by brain region.

KEYWORDS

aerobic glycolysis, aging, carbon-13, lactate, metabolism, MRI, parcellation

---

Abbreviations: ANOVA, analysis of variance; B_p, bicarbonate-to-pyruvate ratio; CBF, cerebral blood flow; CMRO2, cerebral metabolic rate of oxygen consumption; FDG, fluorodeoxyglucose; FSL, FMRIB software library; ID, identification; L_B, lactate-to-bicarbonate ratio; L_p, lactate-to-pyruvate ratio; MCT, monocarboxylate transporter; MRI, magnetic resonance imaging; MRS, magnetic resonance spectroscopy; OGI, oxygen–glucose index; PET, positron emission tomography.

....

1 | INTRODUCTION

Aging is associated with well documented changes in brain physiology and cognitive performance (López-Otín et al., 2013). Cerebral blood flow (CBF) tends to decrease in the brain with age, while the rate of oxygen consumption (CMR02) increases slightly (Hanzhang et al., 2011), resulting in a net decrease in venous oxygenation. Imaging with fluorodeoxyglucose positron emission tomography ([^{18}F] FDG-PET) has demonstrated a 7% per decade decrease in FDG uptake with age (Greve et al., 2016).

These changes in oxygen consumption versus age are consistent with decreasing usage of glucose in nonoxidative metabolic pathways and/or increasing usage of alternative energy substrates such as ketones in the brain with age. Glucose can be metabolized nonoxidatively via lactate production as well as the nonoxidative branch of the pentose-phosphate pathway. The degree of nonoxidative metabolism of glucose has been estimated in vivo using the oxygen–glucose index (OGI) (the ratio between $^{15}O_2$ and ^{18}F-FDG uptake measured with PET). The OGI has been shown to be less than 6.0 (the value for purely oxidative glucose metabolism) throughout much of the brain and varies regionally (Vaishnavi et al., 2010). The OGI increases throughout the brain as a part of physiological aging (Goyal et al., 2017). Whether or not this change is mainly due to decreasing lactate production in the brain, as hypothesized by Goyal et al. (2017), is still under investigation (Drulis-Fajdasz et al., 2018).

Lactate plays an important role in the brain (Pellerin et al., 1998), as it is involved in neuroprotection during ischemia (Castillo et al., 2015), the formation of long-term memories (Suzuki et al., 2011), hippocampal neurogenesis (Lev-Vachnish et al., 2019), and signaling (Magistretti & Allaman, 2018). Current methods for probing lactate production in the human brain, namely proton magnetic resonance spectroscopy (MRS) to measure the lactate pool size or PET to measure the OGI, provide an incomplete picture. Proton MRS can be used to measure the net lactate concentration, which does increase locally during brain activation (Koush et al., 2019, 2021; Mangia et al., 2006). The OGI reflects the relative rate of all nonoxidative uses of glucose, which includes lactate production and other fates.

In this study, HP-^{13}C MRI was used to measure ^{13}C-metabolite signals in a cohort of 35 cognitively normal individuals to investigate global and regional changes in ^{13}C-metabolite production with age. This recently developed method enables imaging of the conversion of ^{13}C-labeled substrates into downstream ^{13}C-labeled metabolites, such as the conversion of ^{13}C-pyruvate to ^{13}C-lactate or ^{13}C-bicarbonate. The relative signal from each downstream ^{13}C-labeled metabolite provides information about the chain of events that results in that downstream metabolite. Thus ^{13}C-lactate signal is a marker of the anaerobic conversion of ^{13}C-pyruvate to ^{13}C-lactate, while ^{13}C-bicarbonate signal is a marker of ^{13}C-pyruvate conversion to acetyl-CoA. The major rate-limiting factors for these reactions include the transmembrane transport of pyruvate and lactate through monocarboxylate transporters, the local availability of the required enzymes and co-factors, as well as the enzyme activities and pre-existing metabolite concentrations. We hypothesized that ^{13}C-lactate signal would decrease with age in parallel to the decreasing OGI observed using PET imaging (Goyal et al., 2017).

2 | MATERIALS AND METHODS

The cohort consisted of 35 individuals (male: 14, female: 21) ranging in age from 21 to 77. All but one of the participants were screened using the Montreal Cognitive Assessment (MoCA) to exclude individuals with cognitive impairment. The study was conducted under a protocol approved by the Research Ethics Board of Sunnybrook Health Sciences Centre and approved by Health Canada as a Clinical Trial Application. Informed written consent was provided by all participants.

2.1 | Scan workflow

The experimental workflow and the image postprocessing used for data analysis is shown in Figure 1. A General Electric SPINLab polarizer system (GE, Waukesha, WI) was used to polarize each 1.47 g sample of [1-^{13}C]pyruvic acid (Sigma Aldrich, St. Louis, MO) as previously described (Lee et al., 2020). Prior to scanning, a 20-gauge intravenous catheter was inserted into the forearm of each participant to allow for the injection. The volume for injection was preset based on a dose of 0.43 mL/kg of the 250 mM hyperpolarized [1-^{13}C]pyruvate solution.

Participants were positioned within a GE MR750 3.0T MRI scanner (GE Healthcare, Waukesha, WI) with a custom-built ^{13}C head coil (26 cm diameter, 25 cm long, 8-rung lowpass birdcage). The dose of hyperpolarized ^{13}C-pyruvate was injected at 4 mL/s, followed by a 20 mL saline flush at 5 mL/s. Immediately following the flush, whole-brain ^{13}C-lactate, ^{13}C-bicarbonate, and ^{13}C-pyruvate images were acquired every 5 s over a 60 s imaging window, with 1.5 cm isotropic spatial resolution.

Each volume-timepoint was imaged using 24 excitations to encode the 3D volume, with net tip angles of 80° for ^{13}C-lactate, 80° for ^{13}C-bicarbonate, and 11° for ^{13}C-pyruvate (Cunningham et al., 2008; Geraghty et al., 2018). The pulse sequence also included a slab-localized spectroscopy acquisition from a 4 cm thickness axial slab centered on the corpus callosum, applied once each 5 s, after each block of ^{13}C-metabolite imaging. This spectroscopy data were used for quality control of the metabolic image acquisitions.

After the ^{13}C imaging and spectroscopy were collected, the participants remained in the scanner in the same position, while the ^{13}C head coil was replaced with an 8-channel ^{1}H neurovascular array (Invivo Inc., Pewaukee, WI) to permit standard anatomical imaging (axial fast spoiled gradient echo images, FOV 25.6 × 25.6 cm^2, 1 mm isotropic resolution, TR 7.6 ms, TE 2.9 ms, flip angle 11°). Foam padding was used to minimize head movement between the metabolic and anatomic scans. The ^{13}C-images were reconstructed and resampled in Matlab (MATLAB, 2019) and saved in DICOM format for further analysis.
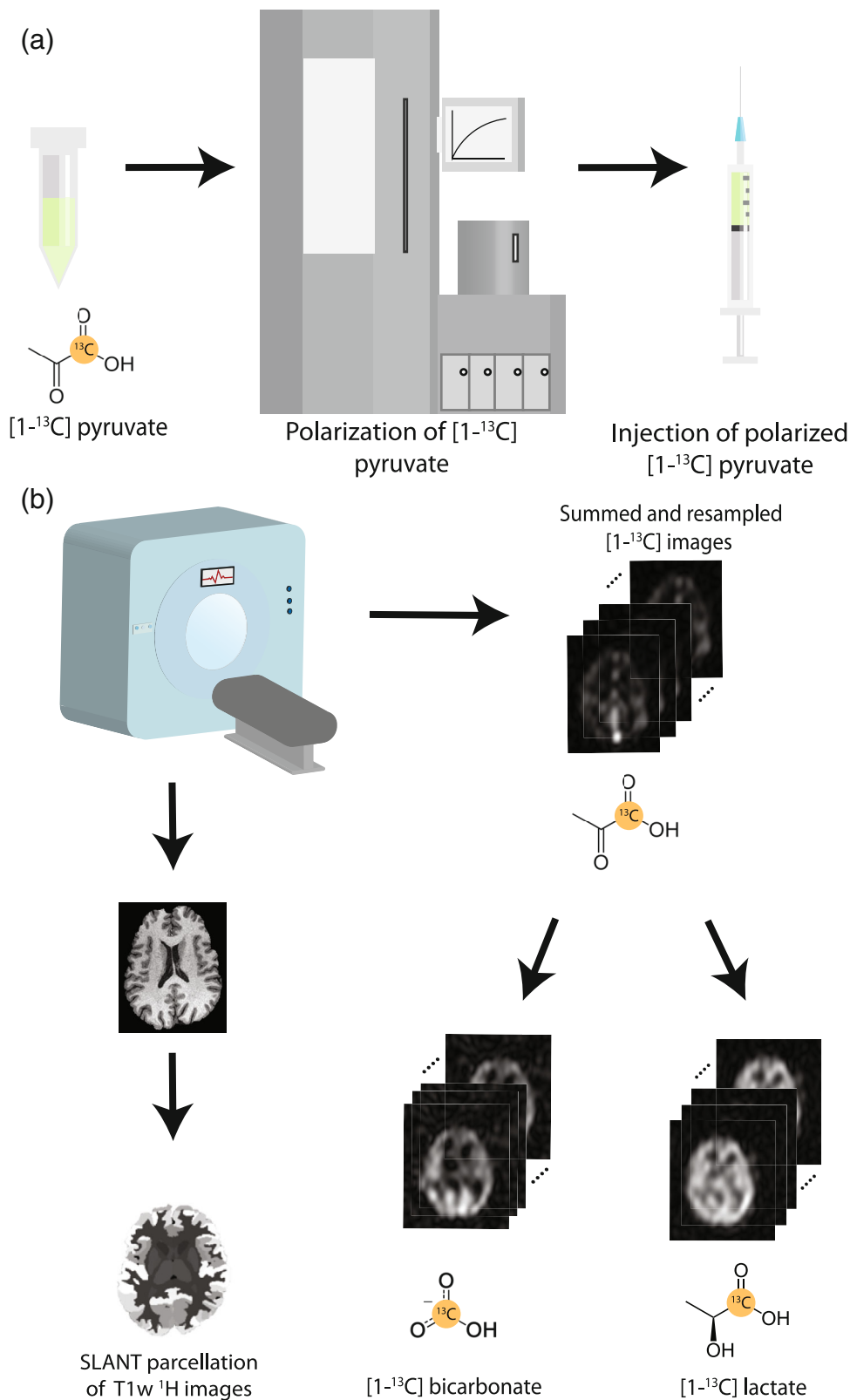
(a)

[1-^{13}C] pyruvate

Polarization of [1-^{13}C] pyruvate

Injection of polarized [1-^{13}C] pyruvate

FIGURE 1 Schematic of the experiment workflow used. (a) Prior to injection, [1-^{13}C]pyruvate is polarized for up to 3 h prior to dissolution and release by a pharmacy technician. (b) The ^{13}C image acquisition starts at the end of injection of polarized ^{13}C-pyruvate and ^{13}C-metabolite images covering the whole brain are acquired. Then conventional anatomical images are acquired, which are parcellated into 132 regions during postprocessing. The parcellation maps are then used to compute mean ^{13}C-metabolite signals for each atlas region.

(b)

Summed and resampled [1-^{13}C] images

SLANT parcellation of T1w ^{1}H images

[1-^{13}C] bicarbonate

[1-^{13}C] lactate

2.2 | Regional metabolite signal normalization

The regional ^{13}C-metabolite signals were computed using the Brain-COLOR labeling protocol (Klein & Tourville, 2012). First, the T1-weighted images were parcellated using the SLANT (Spatially Localized Atlas Network Tiles) method (Huo et al., 2019), providing 132 regions for each participant. The ^{13}C-lactate images were registered to the corresponding T1-weighted images with an affine
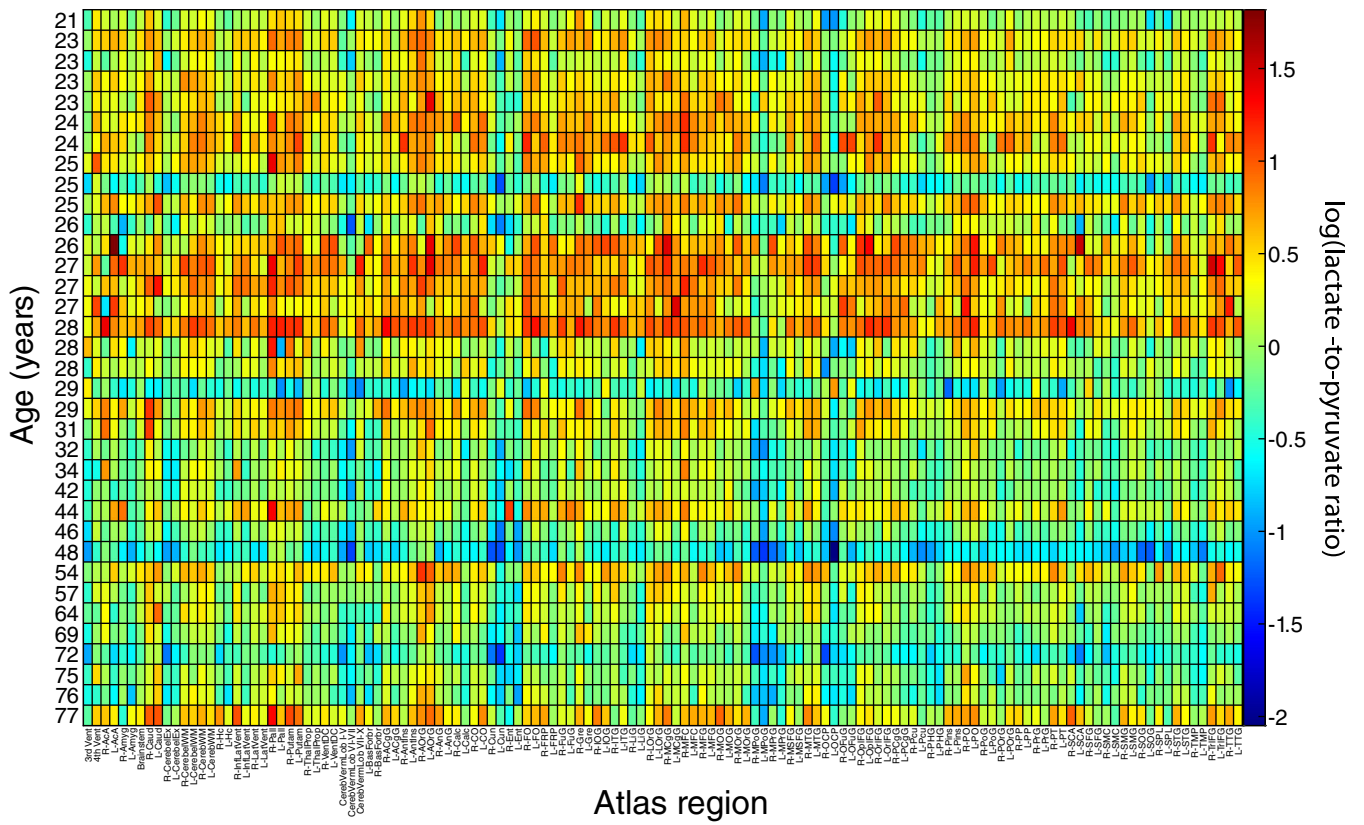
FIGURE 2 Heatmap of the log transformed lactate-to-pyruvate ratio, $\log(L_p)$, for each atlas region, with age on the vertical axis and the BrainCOLOR atlas region across the horizontal axis.
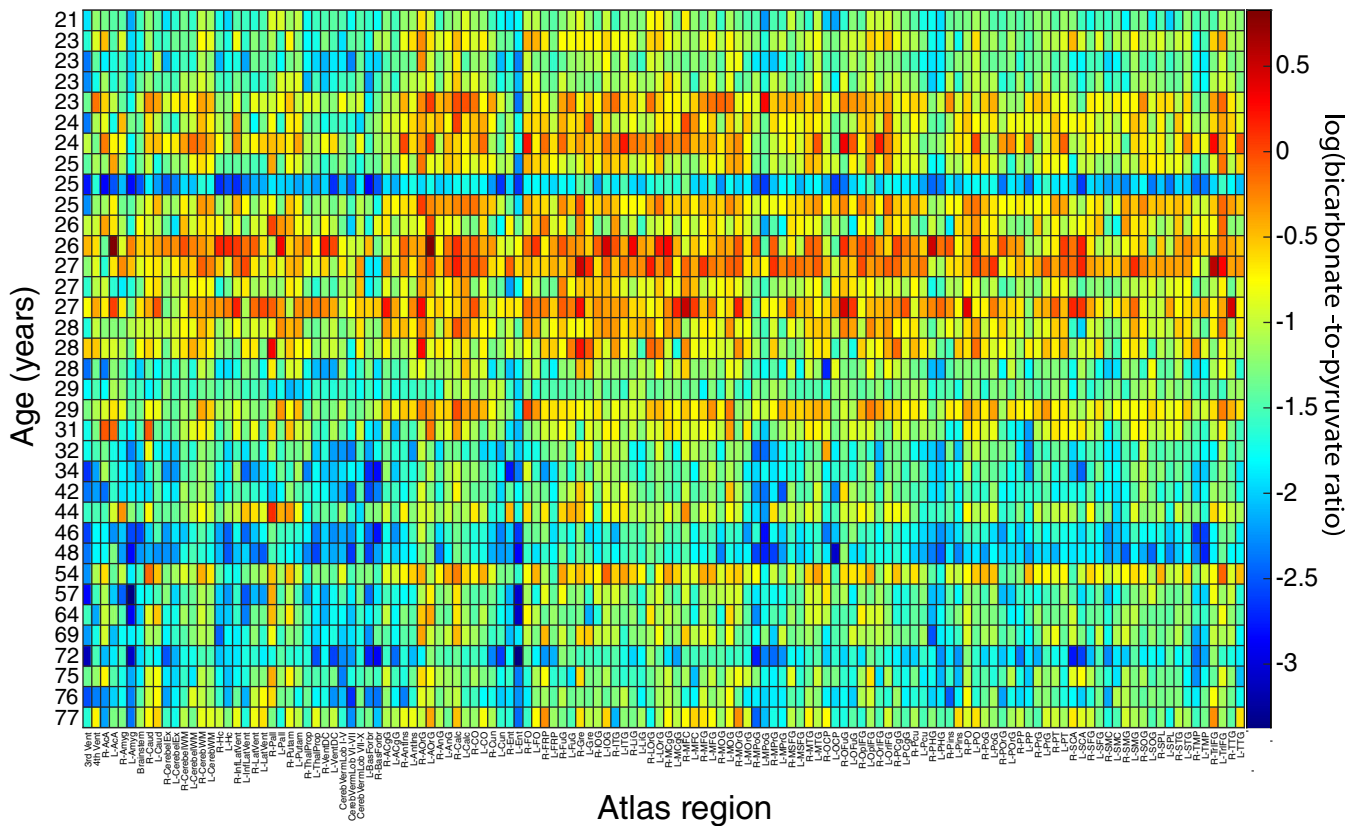

FIGURE 3 Heatmap of the log transformed bicarbonate-to-pyruvate ratio, $\log(B_p)$, for each atlas region, with age on the vertical axis and the BrainCOLOR atlas region label across the horizontal axis.

registration using FSL (Jenkinson et al., 2002). The resulting transformation matrix was then used to register the corresponding ^{13}C-bicarbonate and ^{13}C-pyruvate images for each participant. The participant-specific parcellation map was used to compute the mean ^{13}C-pyruvate, ^{13}C-lactate, and ^{13}C-bicarbonate signal for each region in each participant.

To normalize for the variable polarization of the ^{13}C-pyruvate substrate at the time of delivery, each regional ^{13}C-metabolite signal was integrated over the 12 timepoints and divided by the time integral of the ^{13}C-pyruvate in the same region, giving the lactate-to-pyruvate ratio (L_P), bicarbonate-to-pyruvate ratio (B_P), and lactate-to-bicarbonate ratio (L_B) for each region and participant.

The spectroscopy data were phased and baseline corrected using the SAGE spectral processing package (GE Healthcare). The 12 timepoints were summed together to produce spectra for comparison to the imaging data.

2.3 | Statistical analysis

The analysis was performed on the logarithm transform of L_P, denoted as $\log(L_p)$, to produce a more homoscedastic residual distribution, (see e.g., Figure S12). This was also done for B_P.

Initial mixed-effects ANOVAs were performed for dependent variables $\log(L_p)$ and $\log(B_p)$ with age categorized as "young" or "old" (below or above the median age), and brain region and age–region interaction as the independent variables to establish that these effects were significant.

Post hoc pairwise comparisons of estimated marginal means (Lenth, 2022) were done between the "young" and "old" groups for each of the 132 brain regions. The false-discovery rate method (Benjamini & Hochberg, 1995) was used to adjust the threshold for significance, accounting for the 132 comparisons. Brain regions with a significant *p*-value after this procedure are listed in Tables S6 and S7.
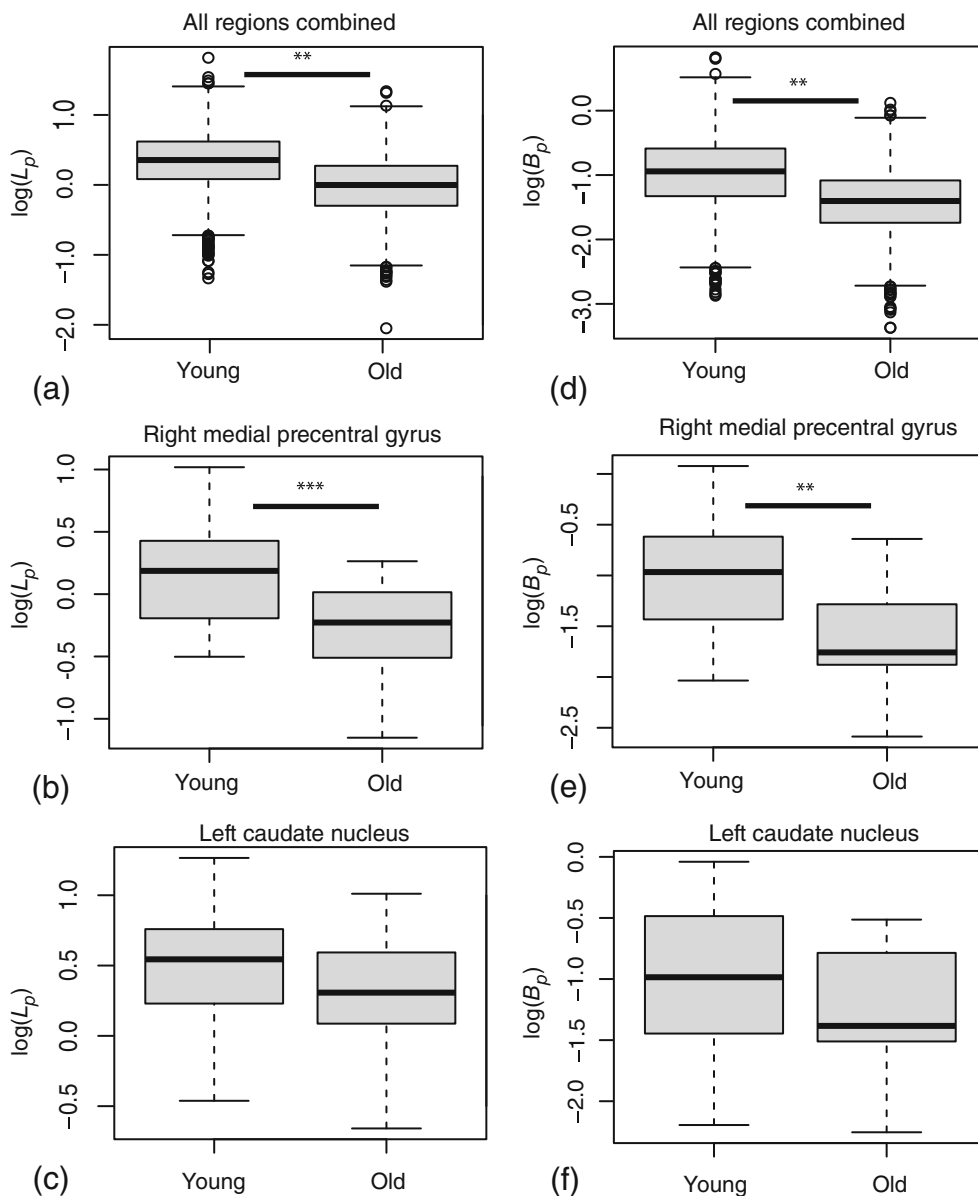

FIGURE 4 Box plots showing the log transformed lactate-to-pyruvate ratio for all regions (a) with age categorized as "young" or "old." The midline shows the median value, the upper and lower limits of the box show the third and first quartile (75th and 25th percentile), respectively. The whiskers show 1.5 times the interquartile range and any data beyond that is plotted as a point. The plots for the two example regions shown in Figure 6 are shown in (b) and (c). The corresponding plots for bicarbonate-to-pyruvate ratio (d–f). **: $p < .01$, ***: $p < .001$.
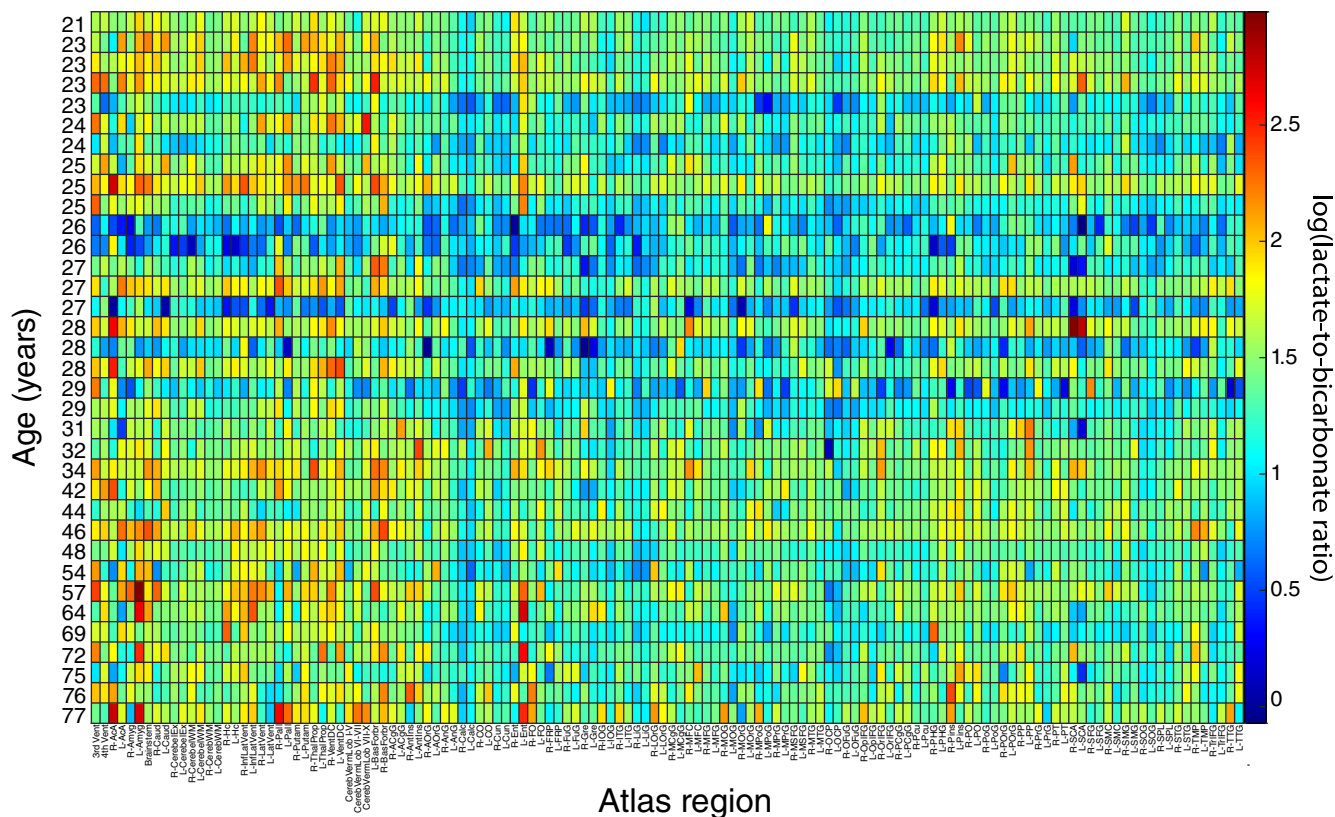
FIGURE 5 Heatmap of the log transformed lactate-to-bicarbonate ratio, $\log(L_B)$, for each atlas region, with age on the vertical axis and the BrainCOLOR atlas region across the horizontal axis.
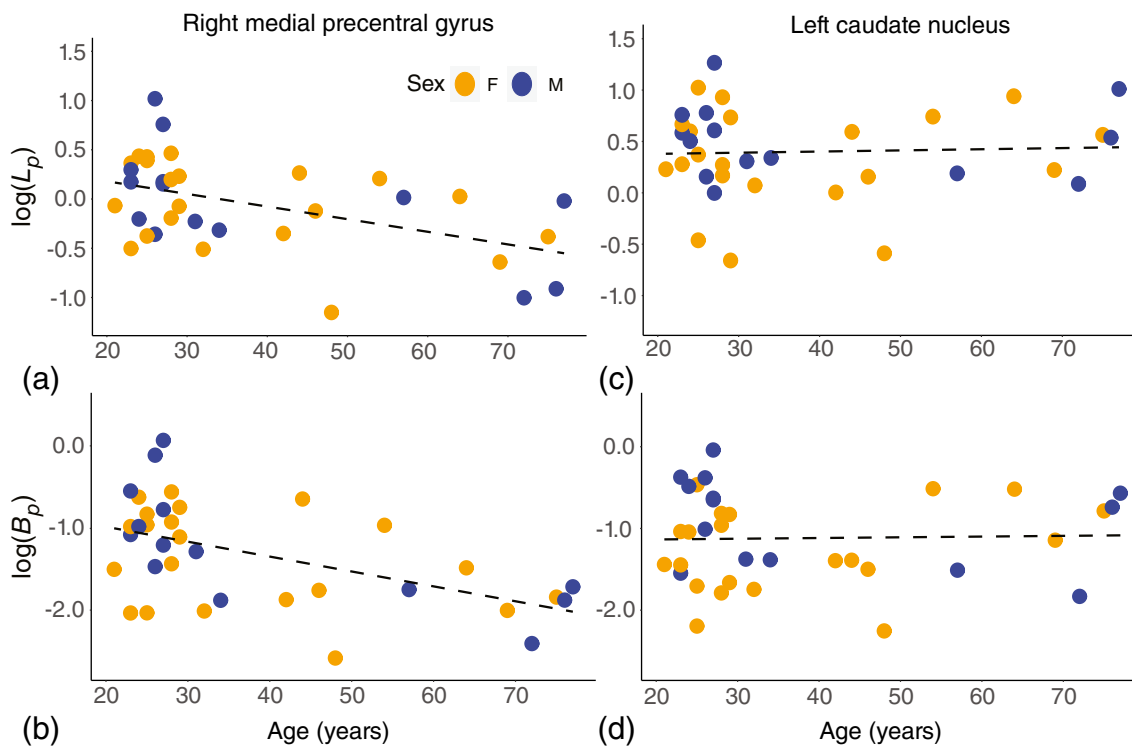

FIGURE 6 Scatter plots of the brain regions with the greatest and least change in both L_P and B_P. The measured values for $\log(L_p)$ and $\log(B_p)$ are shown as dots and the fitted regression line for each region as a dashed line. Each point is color-coded by the sex of the corresponding participant. The y-intercept was computed from the mean of all participant ID beta coefficients plus the intercept coefficient from the regression model. The steepest slope with age for both (a) $\log(L_p)$ and (b) $\log(B_p)$ was observed in the right medial precentral gyrus. The left caudate nucleus showed a flat L_P versus age (c) and B_P that was slightly increasing (d).
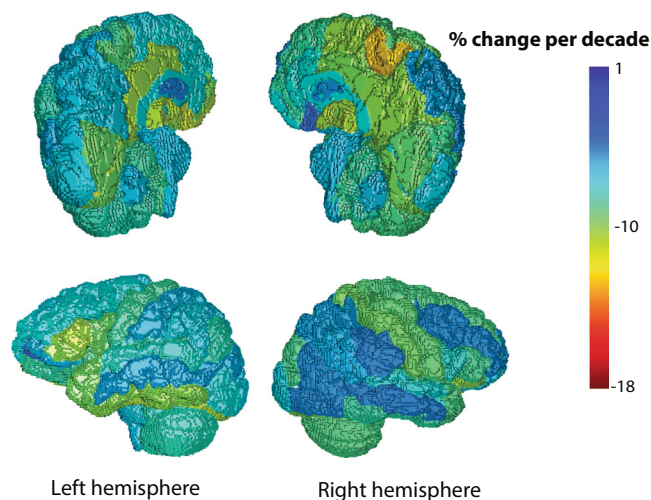
FIGURE 7 The fitted regression model was used to compute a percent change in L_P per decade for each region, displayed as a color on the rendering.
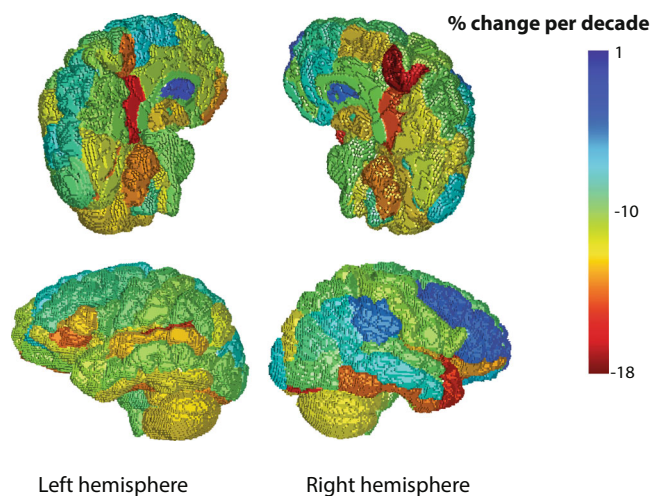

FIGURE 8 The fitted regression model was used to compute a percent change in B_P per decade for each region, displayed as a color on the rendering.

To further explore the details of lactate dependence on age and region, $\log(L_p)$ and $\log(B_p)$ were also analyzed with linear mixed-effects regression in R (version 3-3 using the nlme package [R Core Team et al., 2013]). This form of regression was chosen because multiple measurements from each individual were being analyzed. The regression was repeated for $\log(B_p)$.

The independent variables were added one by one, with models of increasing complexity compared using ANOVA to test whether each independent variable accounted for any additional variance. Biological sex and body weight were not found to explain any additional variance and were thus not included (see Tables S2 and S3). The random effect (participant ID) term was included to account for baseline metabolite levels on administration and other between-participant differences. An age–region interaction term was included to explore how the regional age effect differed from the mean age effect, and

was found to be a statistically significant source of the observed variance.

Once fit, the mixed-effects regression coefficients were used to compute regional percent change per decade for L_P and B_P (see Supporting Information for equation) and are color coded from lowest to highest in Figure 7 and 8. Note that color-coding of the L_P rendering matches the B_P rendering, and B_P showed more extreme changes than L_P.

An apparent increase in $\log(L_p)$ and $\log(B_p)$, and decrease in $\log(L_B)$ was observed for subjects aged 25–30. This was tested for statistical significance with a secondary mixed-effects ANOVA on the subgroup of participants with age ≤30 years ($N = 20$). Fixed effects in the ANOVA were brain region, and age, categorized as younger (age ≤25) and older (age = 26–30). Participant ID was designated a random effect.

3 | RESULTS

3.1 | Lactate

The log of the L_P ratio is plotted versus region and age in Figure 2. In the plot, there is a notable reduction in $\log(L_p)$ with increasing age, but with an apparent temporary increase for individuals in their late twenties.

The initial mixed-effects ANOVA for $\log(L_p)$ with age categorized as "young" or "old" (below or above the median age), brain region and age–region interaction as the independent variables showed that all three were significant (see Table S4). The corresponding box plots are shown in Figure 4a–c.

The mixed-effects regression of $\log(L_p)$ with age as a continuous variable gave a global age beta coefficient of -0.007 ± 0.003 ($p = .02$) for $\log(L_p)$ which corresponds to a $-7\% \pm 2\%$ change per decade. All reported plus/minus values are based on the standard errors from the regression.

3.2 | Bicarbonate

The log of the B_P ratio is plotted versus region and age in Figure 3. There is a visible reduction in $\log(B_p)$ with increasing age, again with an apparent increase for individuals in their late twenties.

The initial mixed-effects ANOVA for $\log(B_p)$ with age categorized as "young" or "old" (below or above the median age), brain region and age–region interaction as the independent variables showed that all but the age–region interaction were significant (see Table S5). The corresponding box plots are shown in Figure 4d–f.

The mixed-effects regression of $\log(B_p)$ with age as a continuous variable gave a global age beta coefficient of -0.01 ± 0.004 ($p = .01$) for $\log(B_p)$ which corresponds to a $-9\% \pm 4\%$ change per decade.

Figure 5 displays $\log(L_B)$ versus atlas region for all subjects, showing no notable change in this ratio with age, which was supported by the results of the corresponding regression. However, a regional variation in the lactate-to-bicarbonate ratio can be observed in this plot and thus will be explored in future experiments.

3.3 | Regional differences

The mixed-effects regression models provided coefficients for the fitted change per year for each of the 132 brain regions. The coefficients were used to compute the regional percent change per decade. The region with one of the greatest percent changes per decade in log (L_p) and log(B_p), the right medial precentral gyrus, and the region with the smallest percent change per decade in both log(L_p) and log(B_p), the left caudate nucleus, are plotted versus age in Figure 6. Comparison of the region plots highlights the region–age interaction effect that gives different slopes against age for different regions. The map of regional change with age in log(L_p) and log(B_p) are shown in Figures 7 and 8, respectively. Overall, a similar pattern of region-dependent change versus age was observed for both L_P and B_P, with matching regions showing fast and slow change.

Comparing hemispheres, the right medial precentral gyrus showed a $-12\%\pm4\%$ change in L_P per decade and $-16\%\pm7\%$ change in B_P versus the left medial precentral gyrus with $-8\%\pm3\%$ per decade in L_P and $-12\%\pm6\%$ per decade in B_P. The left caudate showed a change of $1\%\pm1\%$ in L_P per decade and $1\%\pm1\%$ in B_P versus the right caudate with $-4\%\pm1\%$ per decade in L_P and $-4\%\pm2\%$ per decade in B_P.

Example images from a mid-saggital slice in a younger and older subject are shown in Figure 9. Note that, the raw (non-normalized)

signal from ^{13}C-lactate and ^{13}C-bicarbonate is significantly lower in the older subject, while the ^{13}C-pyruvate signal is similar. The raw ^{13}C-metabolite signal and log transformed ^{13}C-metabolite ratios measured from the summed whole-brain data are plotted versus age in Figure 10 and are in agreement with the overall decrease measured from the parcellated ^{13}-metabolite data.

3.4 | Spectroscopy

Representative spectroscopy data from a single participant are shown in Figure 11. Besides the metabolites that are typically observed in the brain in studies utilizing [1-^{13}C]pyruvate, [1-^{13}C]aspartate (SNR > 5) was also measurable in 26 of the 35 participants, and [4-^{13}C]aspartate was measurable in 8 participants after summing the spectra from all 12 time points. To our knowledge, these data represent the first observation of pyruvate carboxylation in humans using hyperpolarized ^{13}C MRI.

3.5 | Subjects ≤ 30 years old

The mixed-effects regression on the subgroup of participants with age ≤ 30 ($N = 20$) showed no significant age effect in log(L_p), log(B_p),

FIGURE 9 Representative mid-saggital slice from a younger (23 years old [y.o.]) and older (72 y.o.) subject. The color overlay indicates the raw (non-normalized) ^{13}C-lactate (upper row), ^{13}C-bicarbonate (middle row), or ^{13}C-pyruvate (lower row) signal. Lower signal is apparent for both ^{13}C-lactate and ^{13}C-bicarbonate in the older subject (note the color scale), whereas the ^{13}C-pyruvate signal is similar. The bright object (arrows) is the ^{13}C-urea reference used for prescan calibration.
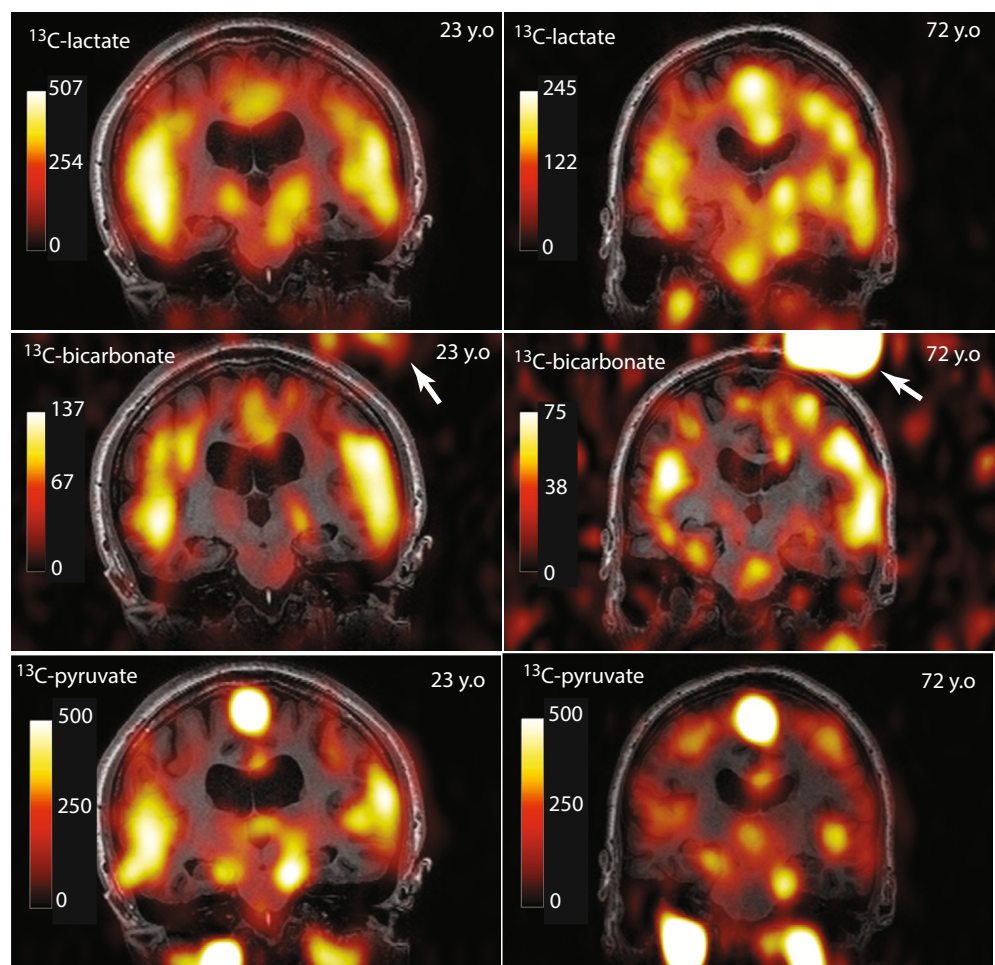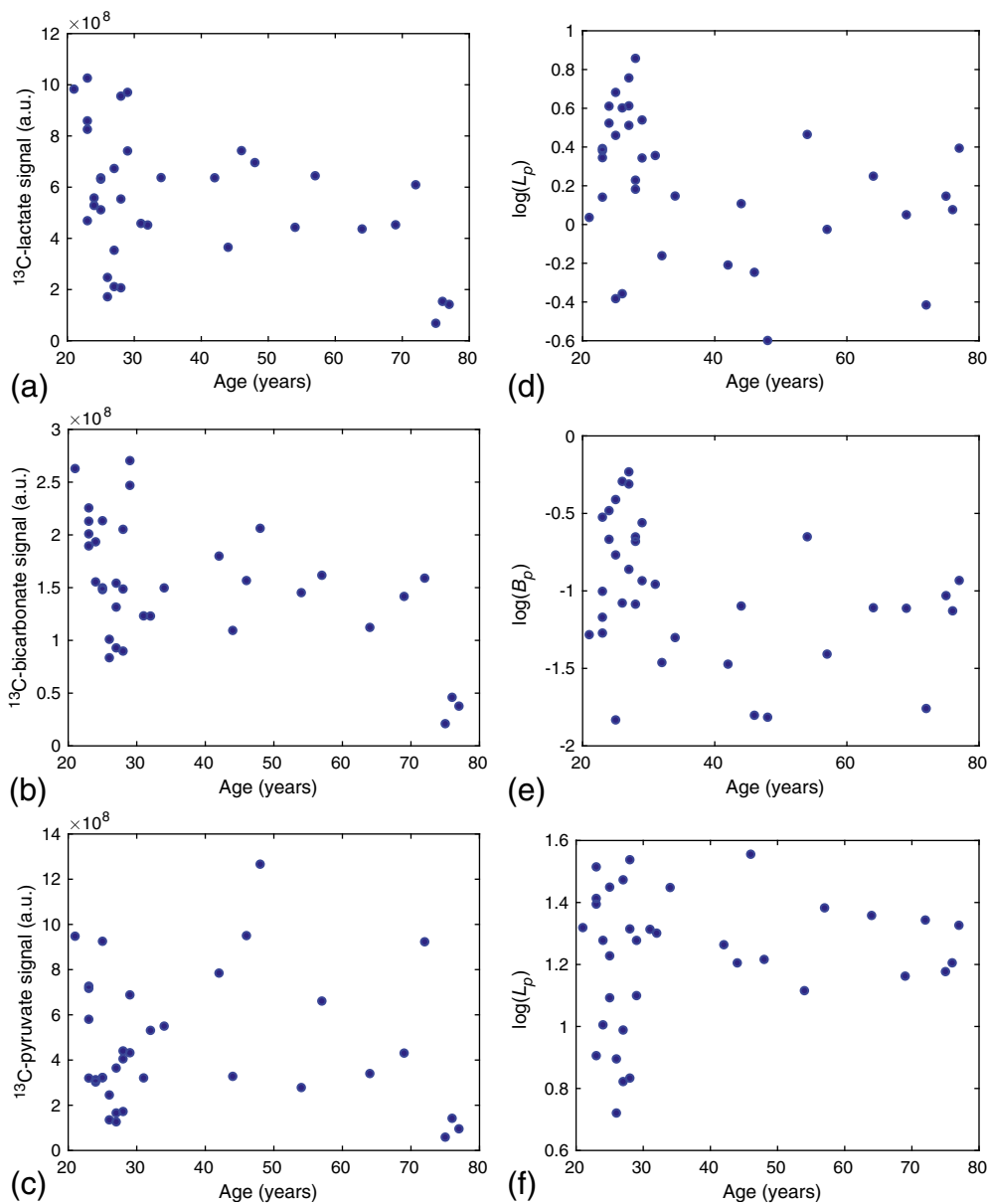
FIGURE 10 Summed whole-brain ^{13}C-metabolite signal versus age. The raw ^{13}C-lactate signal (a) and ^{13}C-bicarbonate signal (b) display a trend toward lower values with increasing age. The ^{13}C-pyruvate signal does not show this trend. The log signal ratios (d–f) computed from the whole-brain signals are in agreement with those from the parcellated results, with a trend toward lower values with increasing age for L_P (d) and B_P (e), and absence of a downward trend for L_B (f).

or $\log(L_B)$. However, $\log(B_p)$ and $\log(L_B)$ had a significant age–region interaction term ($p = .0002$ and $p < .0001$, respectively), suggesting that opposing directions of change among different brain regions may have caused a crossing effect, producing no net age on average.

4 | DISCUSSION

In this study, hyperpolarized ^{13}C-MRI was used to measure ^{13}C-lactate and ^{13}C-bicarbonate production in 132 brain regions versus age. Evidence of decreasing ^{13}C-lactate and ^{13}C-bicarbonate production was found, as reflected by significant negative regression coefficients for both L_p and B_p versus age, with significant differences in this aging effect between brain regions.

The observed reduction in ^{13}C-lactate production with age is consistent with the decreasing FDG uptake and glucose to oxygen ratio versus age observed with PET (Goyal et al., 2017). With both methods, regions of the cerebral cortex like the medial precentral gyrus were among the fastest decreasing regions, while regions of the striatum like the left caudate had minimal change with age.

Reduced CBF with aging (Hanzhang et al., 2011), which would cause reduced vascular ^{13}C-pyruvate signal and/or reduced ^{13}C-pyruvate delivery to the brain, does not explain an age-related decrease in L_P or B_P because ^{13}C-pyruvate signal is in the denominator. It is possible that an age-related increase in blood–brain barrier permeability contributed to increased ^{13}C-pyruvate uptake in some older subjects (Verheggen et al., 2020). However, raw ^{13}C-lactate and ^{13}C-bicarbonate signal showed a decrease with age (Figure 10).
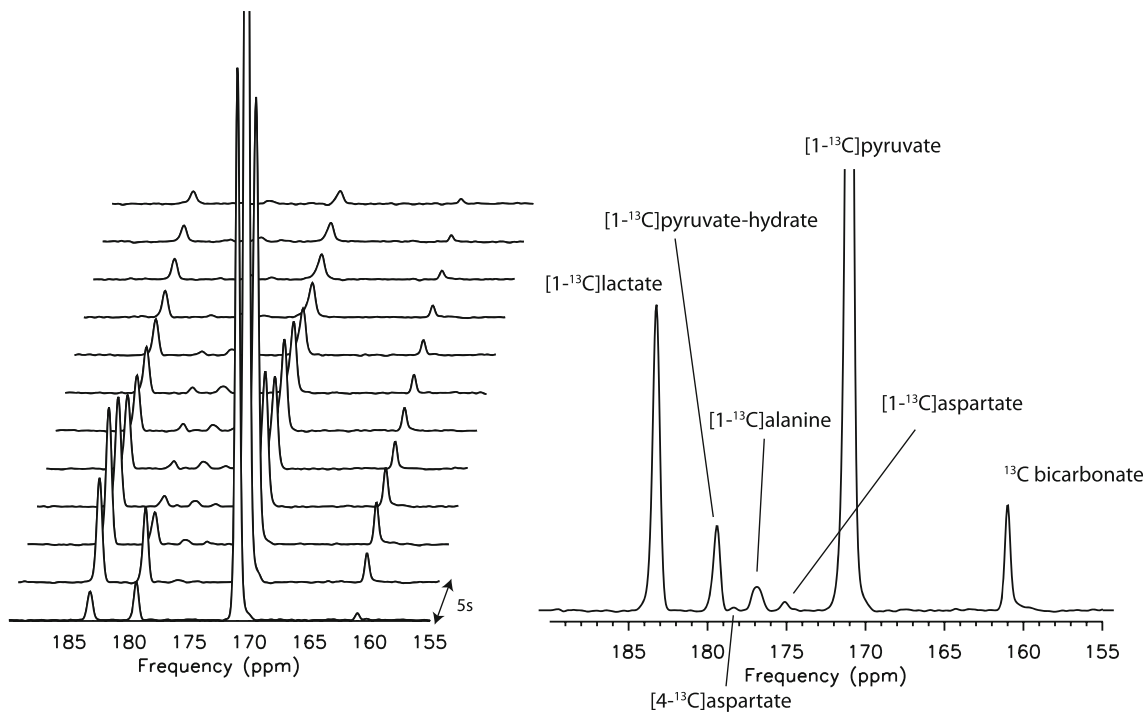
FIGURE 11 Representative spectroscopy data from one participant. Spectra were acquired every 5 s, separately plotted (left) and summed (right). Note the peaks from [1-^{13}C]aspartate and [4-^{13}C]aspartate, indicative of pyruvate carboxylation in the brain.

The conversion of ^{13}C-pyruvate to ^{13}C-lactate has been shown to be dominated by the "exchange-of-label" effect in some conditions, where the steady-state lactate pool size prior to the ^{13}C-pyruvate is injected is the main determinant of the observed ^{13}C-lactate signal (Day et al., 2007). However, the steady-state lactate concentration in the human brain measured by proton spectroscopy is low (0.3–1 mM) (Merboldt et al., 1992; Prichard et al., 1991) and increases with age (Grachev & Apkarian, 2000). Thus, any lactate pool-size effect would be expected to increase with age and does not explain the observed reduction in ^{13}C-lactate production. Nor does it explain the age-associated reduction in ^{13}C-bicarbonate, which is produced in an irreversible reaction within mitochondria (Merritt et al., 2007) and thus not subject to the exchange phenomenon.

The fact that ^{13}C-bicarbonate production decreased with age in most brain regions largely in proportion to the reduction in ^{13}C-lactate production was not anticipated. A hypothesis for why these two signals change in tandem is that the reduction in ^{13}C-lactate and ^{13}C-bicarbonate production with age are caused by a change in a common pathway involving lactate production and matched consumption.

The limitations of the study include the spatial resolution of the ^{13}C-metabolite images, which was relatively coarse (isotropic 1.5 cm voxels), causing partial-volume errors for the smallest regions in the BrainCOLOR atlas. It is likely that the age-associated variation in ^{13}C-metabolite signal in some smaller regions was deemed statistically insignificant due to this source of error. The parcellation was performed automatically without human input and may contain errors. Neither of these issues would change the main findings. The subanalysis of participants of age ≤30 years showed that neither ^{13}C-lactate, nor ^{13}C-bicarbonate production change with age during this specific timeframe. However, this may be an artifact of the limited sample size.

5 | CONCLUSIONS

Hyperpolarized ^{13}C MRI was used to measure regional ^{13}C-lactate and ^{13}C-bicarbonate production in a healthy aging cohort. A significant global decrease in both ^{13}C-lactate and ^{13}C-bicarbonate production with age was observed. A mixed effects linear regression analysis identified regions that were changing with a significantly higher or lower rate with age than the mean global change. These findings are in agreement with the PET literature showing decreasing glucose uptake and nonoxidative glucose consumption with increasing age and supports the hypothesis that this is due to decreasing lactate production in the brain with age.

AUTHOR CONTRIBUTIONS

Casey Y. Lee, Benjamin Geraghty, Albert P. Chen, and Charles H. Cunningham developed the data acquisition methods. Biranavan Uthayakumar, Nadia D. Bragagnolo, Nicole I. C. Cappelletto, Casey

Y. Lee, and Ruby Endre operated the MRI scanner. Biranavan Uthayakumar, Casey Y. Lee, and Benjamin Geraghty did the image reconstruction. Biranavan Uthayakumar did the image analysis. Hany Soliman assessed the participants and performed the ^{13}C-pyruvate injections. Ruby Endre operated the injector. William J. Perks and Nathan Ma performed compounding and pharmacy release of the ^{13}C-pyruvate doses. Albert P. Chen and Charles H. Cunningham built the ^{13}C head coil. Chris Heyn and Sandra E. Black interpreted the images. All authors critically reviewed and edited the manuscript.

DATA AVAILABILITY STATEMENT

The data that support the findings of this study are available from the corresponding author upon reasonable request.

ORCID

Bradley J. MacIntosh https://orcid.org/0000-0001-7300-2355
Charles H. Cunningham https://orcid.org/0000-0001-9636-8130

REFERENCES

Benjamini, Y., & Hochberg, Y. (1995). Controlling the false discovery rate: A practical and powerful approach to multiple testing. *Journal of the Royal Statistical Society: Series B (Methodological)*, *57*(1), 289–300.

Castillo, X., Rosafio, K., Wyss, M. T., Drandarov, K., Buck, A., Pellerin, L., Weber, B., & Hirt, L. (2015). A probable dual mode of action for both l- and d-lactate neuroprotection in cerebral ischemia. *Journal of Cerebral Blood Flow & Metabolism*, *35*(10), 1561–1569.

Cunningham, C. H., Chen, A. P., Lustig, M., Hargreaves, B. A., Lupo, J., Duan, X., Kurhanewicz, J., Hurd, R. E., Pauly, J. M., Nelson, S. J., et al. (2008). Pulse sequence for dynamic volumetric imaging of hyperpolarized metabolic products. *Journal of Magnetic Resonance*, *193*(1), 139–146.

Day, S. E., Kettunen, M. I., Gallagher, F. A., De-En, H., Lerche, M., Wolber, J., Golman, K., Ardenkjaer-Larsen, J. H., & Brindle, K. M. (2007). Detecting tumor response to treatment using hyperpolarized 13C magnetic resonance imaging and spectroscopy. *Nature Medicine*, *13*(11), 1382–1387.

Drulis-Fajdasz, D., Gizak, A., Wójtowicz, T., Wiśniewski, J. R., & Rakus, D. (2018). Aging-associated changes in hippocampal glycogen metabolism in mice. Evidence for and against astrocyte-to-neuron lactate shuttle. *Glia*, *66*(7), 1481–1495.

Geraghty, B. J., Lau, J. Y. C., Chen, A. P., & Cunningham, C. H. (2018). Dual-echo EPI sequence for integrated distortion correction in 3d time-resolved hyperpolarized 13c MRI. *Magnetic Resonance in Medicine*, *79*(2), 643–653.

Goyal, M. S., Vlassenko, A. G., Blazey, T. M., Yi, S., Couture, L. E., Durbin, T. J., Bateman, R. J., Benzinger, T. L.-S., Morris, J. C., & Raichle, M. E. (2017). Loss of brain aerobic glycolysis in normal human aging. *Cell Metabolism*, *26*(2), 353–360.

Grachev, I. D., & Apkarian, A. V. (2000). Chemical heterogeneity of the living human brain: A proton MR spectroscopy study on the effects of sex, age, and brain region. *NeuroImage*, *11*(5), 554–563.

Greve, D. N., Salat, D. H., Bowen, S. L., Izquierdo-Garcia, D., Schultz, A. P., Ciprian Catana, J., Becker, A., Svarer, C., Knudsen, G. M., Sperling, R. A., et al. (2016). Different partial volume correction methods lead to different conclusions: An 18F-FDG-PET study of aging. *NeuroImage*, *132*, 334–343.

Hanzhang, L., Feng, X., Rodrigue, K. M., Kennedy, K. M., Cheng, Y., Flicker, B., Hebrank, A. C., Jinsoo, U., & Park, D. C. (2011). Alterations in cerebral metabolic rate and blood supply across the adult lifespan. *Cerebral Cortex*, *21*(6), 1426–1434.

Huo, Y., Zhoubing, X., Xiong, Y., Aboud, K., Parvathaneni, P., Bao, S., Bermudez, C., Resnick, S. M., Cutting, L. E., & Landman, B. A. (2019). 3d whole brain segmentation using spatially localized atlas network tiles. *NeuroImage*, *194*, 105–119.

Jenkinson, M., Bannister, P., Brady, M., & Smith, S. (2002). Improved optimization for the robust and accurate linear registration and motion correction of brain images. *NeuroImage*, *17*(2), 825–841.

Klein, A., & Tourville, J. (2012). 101 labeled brain images and a consistent human cortical labeling protocol. *Frontiers in Neuroscience*, *6*, 171.

Koush, Y., de Graaf, R. A., Jiang, L., Rothman, D. L., & Hyder, F. (2019). Functional MRS with j-edited lactate in human motor cortex at 4 T. *NeuroImage*, *184*, 101–108.

Koush, Y., de Graaf, R. A., Kupers, R., Dricot, L., Ptito, M., Behar, K. L., Rothman, D. L., & Hyder, F. (2021). Metabolic underpinnings of activated and deactivated cortical areas in human brain. *Journal of Cerebral Blood Flow & Metabolism*, *41*(5), 986–1000.

Lee, C. Y., Soliman, H., Geraghty, B. J., Chen, A. P., Connelly, K. A., Endre, R., Perks, W. J., Heyn, C., Black, S. E., & Cunningham, C. H. (2020). Lactate topography of the human brain using hyperpolarized ^{13}C-MRI. *NeuroImage*, *204*, 116202.

Lenth, R. V. (2022). *emmeans: Estimated marginal means, aka least-squares means*. R package version 1.7.3.

Lev-Vachnish, Y., Cadury, S., Rotter-Maskowitz, A., Feldman, N., Roichman, A., Illouz, T., Varvak, A., Nicola, R., Madar, R., & Okun, E. (2019). L-lactate promotes adult hippocampal neurogenesis. *Frontiers in Neuroscience*, *13*, 403.

López-Otín, C., Blasco, M. A., Partridge, L., Serrano, M., & Kroemer, G. (2013). The hallmarks of aging. *Cell*, *153*(6), 1194–1217.

Magistretti, P. J., & Allaman, I. (2018). Lactate in the brain: From metabolic end-product to signalling molecule. *Nature Reviews Neuroscience*, *19*(4), 235–249.

Mangia, S., Tkáč, I., Gruetter, R., Van De Moortele, P.-F., Giove, F., Maraviglia, B., & Uğurbil, K. (2006). Sensitivity of single-voxel 1H-MRS in investigating the metabolism of the activated human visual cortex at 7 T. *Magnetic Resonance Imaging*, *24*(4), 343–348.

MATLAB. (2019). *Version 7.10.0 (R2019b)*. The MathWorks Inc.

Merboldt, K.-D., Bruhn, H., Hanicke, W., Michaelis, T., & Frahm, J. (1992). Decrease of glucose in the human visual cortex during photic stimulation. *Magnetic Resonance in Medicine*, *25*(1), 187–194.

Merritt, M. E., Harrison, C., Storey, C., Jeffrey, F. M., Sherry, A. D., & Malloy, C. R. (2007). Hyperpolarized ^{13}C allows a direct measure of flux through a single enzyme-catalyzed step by NMR. *Proceedings of the National Academy of Sciences*, *104*(50), 19773–19777.

Pellerin, L., Pellegri, G., Bittar, P. G., Charnay, Y., Bouras, C., Martin, J.-L., Stella, N., & Magistretti, P. J. (1998). Evidence supporting the existence of an activity-dependent astrocyte-neuron lactate shuttle. *Developmental Neuroscience*, *20*(4–5), 291–299.

Prichard, J., Rothman, D., Novotny, E., Petroff, O., Kuwabara, T., Avison, M., Howseman, A., Hanstock, C., & Shulman, R. (1991). Lactate rise detected by 1H NMR in human visual cortex during physiologic

stimulation. *Proceedings of the National Academy of Sciences of the United States of America*, *88*(13), 5829–5831.

R Core Team. (2013). *R: A language and environment for statistical computing*.

Suzuki, A., Stern, S. A., Bozdagi, O., Huntley, G. W., Walker, R. H., Magistretti, P. J., & Alberini, C. M. (2011). Astrocyte-neuron lactate transport is required for long-term memory formation. *Cell*, *144*(5), 810–823.

Vaishnavi, S. N., Vlassenko, A. G., Rundle, M. M., Snyder, A. Z., Mintun, M. A., & Raichle, M. E. (2010). Regional aerobic glycolysis in the human brain. *Proceedings of the National Academy of Sciences*, *107*(41), 17757–17762.

Verheggen, I., de Jong, J. J. A., van Boxtel, M. P. J., Gronenschild, E. H. B. M., Palm, W. M., Postma, A. A., Jansen, J. F. A., Verhey, F. R. J., & Backes, W. H. (2020). Increase in blood–brain barrier leakage in healthy, older adults. *Geroscience*, *42*(4), 1183–1193.

SUPPORTING INFORMATION

Additional supporting information can be found online in the Supporting Information section at the end of this article.